Cancer Imaging

https://doi.org/10.1186/s40644-026-01003-1

Article in Press

Cancer predisposition syndromes: an imaging review

Received: 29 November 2025

Accepted: 5 February 2026

Published online: 17 February 2026

Cite this article as: Mertiri L., Tran H.B., Mertiri D. *et al.* Cancer predisposition syndromes: an imaging review. *Cancer Imaging* (2026). https://doi.org/10.1186/s40644-026-01003-1

Livja Mertiri, Huy Brandon Tran, Denada Mertiri, Maarten Lequin, Nilesh K. Desai & Thierry A. G. M. Huisman

Cancer Predisposition Syndromes: An Imaging Review

Livja Mertiri[1], Huy Brandon Tran[1], Denada Mertiri[2], Maarten Lequin[1], Nilesh K. Desai[1], Thierry A.G.M. Huisman[1]

1. Edward B. Singleton Department of Radiology, Texas Children's Hospital and Baylor College of Medicine, Houston, Texas, USA
2. Faculty of Medicine and Surgery, Università di Tor Vergata, Rome, Italy

Corresponding Author:

Livja Mertiri, MD

Edward B. Singleton Department of Radiology

Texas Children's Hospital and Baylor College of Medicine

6701 Fannin Street, Suite 470

Houston, TX 77030

Phone: +1 832 822-5363

Fax: +1 832 825-0160

Email: lxmertir@texaschildrens.org

KEYWORDS: Cancer Predisposition Syndromes; Neurofibromatosis type 1; Neurofibromatosis type 2; von Hippel-Lindau disease; PTEN - hamartoma tumor syndrome; Beckwith-Wiedemann syndrome; Multiple endocrine neoplasia.

Abstract

Background

Cancer predisposition syndromes (CPSs) are inherited disorders that increase the risk of developing cancer from childhood through adulthood. They account for up to 10% of pediatric tumors, making early recognition important for reducing morbidity and mortality. Because these syndromes show variable penetrance and a wide range of clinical presentations even within the same family, identifying affected children can be challenging.

Main Body

Imaging is an essential tool for diagnosis, surveillance and follow-up of children with cancer predisposition syndromes. In this review we summarize the main clinical and imaging features of Neurofibromatosis type 1, Neurofibromatosis type 2, von Hippel–Lindau disease, PTEN-hamartoma tumor syndrome, Beckwith–Wiedemann syndrome, and multiple endocrine neoplasia. The goal is to help radiologists and clinicians identify these conditions earlier and improve patient care.

Conclusion

A clear understanding of the clinical and imaging features of cancer predisposition syndromes can support earlier identification, closer surveillance, and improved outcomes. Radiologists play a crucial role in

recognizing characteristic patterns and guiding timely management for affected children and their families.

Cancer Predisposition Syndromes: an imaging review

1. Introduction

Cancer predisposition syndromes (CPSs) are a group of inherited disorders that significantly increase the lifetime risk of developing cancer. They account for up to 10% of all childhood tumors, making appropriate surveillance essential to reduce morbidity and mortality. Family cancer history, age, presence of a specific tumor pattern (tumor type and laterality) should be considered when evaluating whether a child may have genetic predisposition [1]. In addition to genetic testing, imaging is now an essential tool for diagnosis, surveillance and follow-up of individuals with suspected or confirmed CPS.

These syndromes show highly variable clinical manifestations, with marked heterogeneity even within families with a shared mutation. CPSs with a particular focus on head and neck imaging findings have been previously described [2]. The purpose of the present article is to complement that prior work by focusing on CPSs that affect multiple organ systems and are frequently encountered in pediatric and adult radiology practice. Specifically, we review the general imaging findings of Neurofibromatosis type 1, Neurofibromatosis type 2, von Hippel-Lindau disease, PTEN-hamartoma tumor syndrome, Beckwith-Wiedemann syndrome, and multiple endocrine neoplasia. We provide a background summary describing genetics and clinical presentations, followed by a detailed description of the imaging findings of the most common associated benign and malignant

lesions. CPSs already reviewed in our prior head and neck–focused article [2] are not covered in this article.

2. Neurofibromatosis Type 1

Neurofibromatosis type 1 (NF1) is an autosomal dominant genetic disorder caused by mutations in the NF1 gene, leading to loss of neurofibromin function and consequent activation of the RAS oncogene[3]. Approximately half of cases are familial, while the remainder result from de novo mutations [4]. Clinical manifestations vary widely even within the same family and include café au lait macules, Lisch nodules (iris hamartomas), learning disabilities, behavior problems, neurofibromas, malignant peripheral nerve sheath tumors (MPNST), optic and non-optic gliomas, breast cancer, hematologic malignancies, gastrointestinal stromal tumors (GISTs), rhabdomyosarcomas, pheochromocytomas, paragangliomas and stromal tumors. Affected individuals present with a combination of cutaneous, ocular, neurological, and skeletal findings (Table 1) [3]. In young children, the presence of bony abnormalities, café-au-lait macules, plexiform neurofibromas, and optic gliomas raise the suspicion of NF1 [5].

Neurofibromas are benign peripheral nerve sheath tumors that may arise anywhere along the nerves. Dermal and subcutaneous neurofibromas occur in approximately 60% of NF1 patients [6] and commonly manifest as pedunculated papulonodular cutaneous or subcutaneous lesions in young

adults [7]. On ultrasound (US), they appear as well-defined, oval, hypoechoic masses in continuity with a peripheral nerve, and are typically hypovascular on Color Doppler [8].

Plexiform neurofibromas are more complex, firm, superficial or deep masses characterized by longitudinal growth along the nerves, involving multiple fascicles and branches. They may overgrow, infiltrate, and erode adjacent structures [2, 5, 9]. These tumors are pathognomonic for NF1 and occur in 30-50% of patients, usually in infancy or childhood, and most commonly in the craniomaxillofacial region [10, 11]. The ophthalmic branch of the trigeminal nerve is frequently involved and may be associated with sphenoid dysplasia, ductal ectasia and aqueduct stenosis, and buphtalmus [12, 13].

Spinal neurofibromas, in particular those at C2 nerve route, tend to occur bilaterally, and have a high incidence of intradural extension and myelopathy [10]. Large multiple paraspinal neurofibromas are frequently associated with vertebral dysplasia and dystrophic scoliosis [5, 10].

On MRI, plexiform neurofibromas appear as multinodular confluent masses with mass effect and the characteristic target sign on T2-weighted image (WI) (hyperintense peripheral rim and hypointense central fibrous component) (Figure 1). They appear hypointense on T1WI and show variable post-contrast enhancement [5]. Although most plexiform neurofibromas remain benign, the lifetime risk of malignant transformation to MPNST is approximately 10% [14]. Malignant progression is thought to

occur through stepwise accumulation of genetic alterations, with transition from plexiform neurofibromas to atypical neurofibromatous neoplasm of uncertain biological potential (ANNUBP), and ultimately to MPNST following additional mutations [15]. Currently, ANNUBPs are diagnosed on histopathology; however, imaging plays a key role in identifying lesions suspicious for progression and guiding further evaluation [15, 16]. Imaging features suggestive of malignant transformation include large size, peripheral enhancement, perilesional edema-like signal, intratumoral cystic change, ill-defined margins, and adjacent bone destruction. On ^{18}F-FDG PET/CT, a SUVmax >3.5 favors MPNST, whereas benign lesions typically demonstrate lower uptake [9].Sphenoid wing dysplasia is a hallmark osseous abnormality of NF1 and is characterized by hypoplasia of the greater or lesser sphenoid wing, often demonstrated as an absence of the innominate line on radiographs or CT, known as “bare orbit sign”. This results in widening of the orbital fissures, flattening of the posterior aspect of the orbit, exophthalmos and may be associated with meningocele [9, 17].

Scoliosis is the most common bone abnormality in NF1 patients and may be dystrophic or non-dystrophic. Although less frequent, dystrophic scoliosis typically presents at a younger age (6-10 years vs. adolescence), progresses more rapidly, and is associated with a worse prognosis [9, 18]. It usually involves four to six vertebral bodies, most frequently in the lower cervical/upper thoracic spine, and may be associated with vertebral scalloping, neuroforaminal widening, transverse process spindling [9].

Vertebral body scalloping results from adjacent dural ectasia, neurofibromas, or thoracic meningoceles [9, 18].

Dysplasia of the long bones, especially the tibia and fibula, is a less frequent bone abnormality, but represents a characteristic skeletal manifestation of NF1 in infancy. It is usually unilateral and presents in infancy with anterolateral tibial bowing, fractures and pseudoarthrosis due to abnormal bone remodeling [11, 18].

Focal areas of signal intensity (FASI) are a distinguishing imaging finding in children with NF1, and consist of foci of increased T2 and FLAIR signal intensity [10]. They occur in approximately 70% of patients [9], typically appearing by age of 3 years, increasing in number and size until about 10-12 years of age [5], and then typically start regressing; they are rarely seen after age of 20 years [5, 9, 10]. Pathologically, FASI are considered benign lesions and correspond to spongiform myelopathy and myelin vacuolization [19], though rare cases of tumor development within these areas have been reported, supporting the need for MRI surveillance [20]. FASI are typically located in the cerebellum, brainstem, and basal ganglia, and are non-space-occupying, cause no mass effect or clinical symptoms. However, several studies have demonstrated a strong association between FASI – particularly those in the thalamus and cerebellum - and cognitive impairment [21-23]. On MRI, they appear hyperintense on T2WI and FLAIR, are isointense, or occasionally slightly hyperintense on T1WI, and do not enhance after contrast administration.

^{1}H-MRS helps to differentiate FASI from gliomas, as FASI demonstrate near-normal level of N-acetylaspartate [5, 9, 10].

Optic pathway gliomas (OPGs) are the most common central nervous system (CNS) tumors in NF1, occurring in 15-20% of affected children [24]. Most are asymptomatic, but up to 50% of cases may present with poor visual acuity, optic atrophy, visual field defects or papilledema [5]. OPGs typically manifest in young children with median age of 4 years and may develop at any portion of the optic pathway (e.g., optic nerves, chiasm, optic trats, lateral geniculate bodies, optic radiations).

MRI of the brain is the modality of choice to detect OPGs and assess their anatomical extent. OPGs cause enlargement of the optic nerve sheath complex that may appear tubular, fusiform, eccentric or globular with tortuosity [5]. They are hypointense on T1WI, hyperintense on T2WI, and usually enhance after contrast administration (Figure 2) [5, 9, 10]. Fat-saturated sequences improve assessment of optic nerve involvement [5, 27].

Non-optic gliomas occur in approximately 1-2% of NF1 patients and are usually located in the brainstem, cerebellum or spinal cord [5, 10]. Most NF- associated gliomas have a relatively benign course and may even regress [21, 22]. Brainstem gliomas account for approximately 18% of NF1-associated brain neoplasms and occur most commonly in the medulla, followed by the midbrain and pons [5, 28, 29]. Most are asymptomatic, however tectal gliomas may obstruct the aqueduct of Sylvius, leading to hydrocephalus [5, 29]. On MRI, the tectum appear expanded, isointense on

T1WI, and hyperintense on T2WI [5]. Cerebellar gliomas are rare in NF1 patients and usually malignant [5].

GISTs occur in up to 25% of individuals with NF1 [8, 9]. In contrast to the general population, in whom the stomach is the most common site, NF1-associated GISTs more frequently arise in the small bowel and are often multifocal [8]. On imaging, they appear as submucosal wall masses and may demonstrate exophytic, intraluminal, or mixed growth patterns. Areas of low attenuation within the mass on CT suggest hemorrhage and necrosis [8].

Table 1. Diagnostic Criteria for Neurofibromatosis Type 1

- Six or more café-au-lait macules (>5 mm in children and >15 mm in adults)
- Freckling in the axillary or inguinal regions
- Two or more neurofibromas or one plexiform neurofibroma
- Optic pathway glioma
- Two or more Lisch nodules identified by slit lamp examination or two or more choroidal abnormalities
- A distinctive osseous lesion such as sphenoid dysplasia, anterolateral bowing of the tibia, or pseudoarthrosis of a long bone
- A parent with NF1
- A germline NF1 pathogenic variant

Diagnosis of NF1 is made when at least two of these features are identified.

3. Neurofibromatosis Type 2

Neurofibromatosis type 2 (NF2) is an autosomal dominant syndrome caused by loss-of-function mutations in the NF2 tumor suppressor gene, which encodes for merlin, a protein involved in regulating cell growth - particularly in Schwann cells - and cell-cell adhesion [30]. NF2 typically presents in early adulthood and is characterized by multiple inherited schwannomas, meningiomas, and ependymomas (MISME) (Figure 3). Ophthalmologic manifestations and cutaneous involvement occur in approximately 70% of patients [9], whereas neurofibromas are uncommon [31]. Early age at onset and intracranial meningiomas at presentation are associated with increased mortality [32]. Adults most often present with hearing loss, tinnitus, and balance dysfunction due to bilateral vestibular schwannomas, whereas children more frequently exhibit visual disturbances (e.g., cataracts, optic nerve meningiomas, disk gliomas or retinal hamartomas), skin tumors, mononeuropathies [31, 33, 34].

Schwannomas are benign peripheral nerve sheath tumors and represent the most common neoplasms in NF2. They arise most frequently from the vestibular branch of the cranial nerve VIII, and bilateral vestibular

schwannomas are pathognomonic for the disorder [9, 30]. Compared with sporadic lesions, NF2-associated vestibular schwannomas are more aggressive, have a higher mitotic index, and higher risk of recurrence. Disease is typically more aggressive in younger patients [30, 31, 35, 36].

Vestibular schwannomas arise at the neuroglial junction within the internal auditory canal (IAC) and may extend into the cerebellopontine angle if untreated [37]. Large tumors may cause IAC widening, involve the cochlear and facial nerves - resulting in hearing loss or facial paralysis - and compress the brainstem or cerebellum. Severe cases may lead to tonsillar herniation, peritumor edema, or hydrocephalus [37, 38].

In approximately 50% of patients, NF2-associated schwannomas may affect other cranial nerves (most commonly trigeminal and oculomotor nerves) but may also arise from spinal neve roots and peripheral nerves [38, 39].

Distinctive plexiform “plaque-like” dermal or subcutaneous schwannomas may occur in NF2, and together with bilateral vestibular schwannomas or ependymomas, help distinguish NF2 from schwannomatosis [40-42].

On CT, schwannomas appear as isoattenuating masses and, unlike meningiomas, vestibular schwannomas usually do not have calcifications [37]. CT can detect moderate to large lesions, but may miss small intracanalicular tumors [37].

MRI is the preferred diagnostic modality. Brain MRI with thin cuts through the IAC, and in particular sagittal 3D T2WI, provide accurate evaluation of the cochlear nerves [4, 27, 43]. On MRI, schwannomas are hypo- to

isointense on T1WI, hyperintense on T2WI, and demonstrate avid post-contrast enhancement [5]. Larger lesions may demonstrate heterogeneous signal due to intralesional hemorrhage, necrosis, or cystic changes [9, 37].

Meningiomas are the second most common tumors in NF2, and the presence of multiple meningiomas (≈50% of patients) is a major diagnostic criterion for the syndrome [9, 30]. They most frequently occur supratentorially, particularly in the frontal, parietal and temporal regions, and along the falx cerebri [9, 30].

On CT, meningiomas appear as hyperdense dural-based lesions with avid contrast enhancement [5, 44]. On MRI, they are isointense to the gray matter on both T1 and T2WI, and demonstrate homogeneous enhancement with a dural tail [9]. Adjacent skull hyperostosis or erosion may be present [5, 44]. Spinal meningiomas appear as intradural extramedullary masses [9].

Meningioangiomatosis is a rare, benign hamartomatous intracranial lesion, with approximately half of cases associated with NF2 [45]. Pathologically, it is characterized by cortical and leptomeningeal meningovascular proliferation with focal calcifications [5, 45]. In NF2, these lesions are often multiple and asymptomatic, whereas sporadic cases typically present with headaches and seizures [5]. They may be single or multiple, intra-axial or extra-axial, and are most commonly located in the frontal and temporal lobe [45]. On CT, meningioangiomatosis appears as a hypodense, round mass with variable calcifications in the cortical or

leptomeningeal area, demonstrating minimal or no enhancement [45]. On MRI, lesions are usually iso- to hypointense on T1WI, and heterogenous with central hypointensity and surrounding hyperintensity on T2WI [5, 46].

Ependymomas are WHO grade 2 lesions and occur in approximately 53% of individuals with NF2 [30]. Patients often develop multiple spinal cord ependymomas, most commonly in the cervical spinal cord or at cervicomedullary junction, and are usually asymptomatic [30, 47].
On MRI, ependymomas appear as intramedullary tumors, isointense to slightly hyperintense on T1WI and hyperintense on T2WI relative to the normal spinal cord [5, 9]. On post-contrast images they demonstrate intense enhancement and may assume a characteristic aspect of “string of pearls” appearance along the spinal cord or cauda equina [30].

4. Von Hippel–Lindau (VHL) Disease

Von Hippel-Lindau disease is an autosomal dominant multisystem tumor predisposition caused by mutations in the VHL tumor suppressor gene, leading to overexpression of proteins that mediate angiogenesis [3, 48]. The phenotype is highly variable in terms of clinical manifestations and age at onset. Patients may develop multiple benign and malignant tumors, including hemangioblastomas of the retina and CNS, renal cell carcinoma (RCC), pheochromocytoma, neuroendocrine tumors, and renal or pancreatic cysts.

CNS hemangioblastomas are benign WHO grade 1 tumors characterized by a rich capillary network [49]. They form cysts of various size, are often multifocal, and occur most commonly in the cerebellum (≈60%), followed by the spinal cord and brainstem [49, 50]. The mean age of onset is 33 years [50]. Symptoms are usually caused by the associated cysts or syrinx rather than the tumor itself, as these cystic components tend to grow faster and become larger [51]. On CT, hemangioblastomas appear as well defined, homogeneous hypodense cysts with an avidly enhancing mural nodule within the cyst wall [50, 52, 53]. On MRI, the cystic component is typically T1-hypointense and T2-hyperintense, although signal intensity may vary depending on protein content or the presence of hemorrhage (Figure 4) [52, 54]. The solid tumor component shows high T2-signal, abuts the cerebellar surface, and demonstrates marked enhancement on post-contrast T1WI, while the cyst wall does not enhance [50, 52, 53].

Because spinal lesions frequently coexist, spinal MRI should be obtained whenever a cerebellar hemangioblastoma is identified [50, 55]. Close surveillance is recommended, as many tumors exhibit a saltatory growth pattern [55].

The differential diagnosis includes metastases, medulloblastomas, pilocytic astrocytomas, and ependymomas due to the overlapping imaging features. Metastases are usually located at the gray-white matter junction of the surpratentorial brain, show ring enhancement, and are usually multiple

[53]. Pilocytic astrocytomas are typically less vascular and lack flow voids; dynamic susceptibility contrast perfusion-weighted imaging and MR spectroscopy may help in differentiation [56]. Medulloblastomas more frequently arise from the midline cerebellar vermis and present with marked peritumoral edema and restricted diffusion [57]. Ependymomas usually extend from the fourth ventricle into adjacent cisterns and often contain calcifications [57].

Retinal hemangioblastomas develop in 45-60% of VHL patients and the mean age of onset is 25 years [50, 58, 59]. Sometimes they may be the only manifestation of the disease, and in half of the cases are bilateral [50, 59]. On fundoscopy they have a globular appearance with dilated tortuous feeding vessels and optic disc edema, and in 85% of cases they occur in the peripheral retina [60]. The diagnosis is confirmed on ophthalmic examination. Imaging plays a limited role in the diagnosis of retinal hemangioblastomas, however brain MRI may show an enhancing lesion with or without retinal detachment (Figure 5) [50, 61].

Endolymphatic sac tumors are benign but locally invasive neoplasms of the vestibular aqueduct, occurring in approximately 10-15% of individuals with VHL [50]. The mean age at presentation is 22 years, and tumors may be bilateral [50]. Clinical manifestatins include hearing loss, tinnitus, vertigo, and facial nerve palsy [50]. On CT, they demonstrate a moth-eaten appearance of the petrous temporal bone with erosions

involving the vestibular aqueduct, semicircular canals, and cochlea [62, 63]. Central calcific spicules and posterior rim calcifications are frequently noted [62]. On MRI, they appear hyperintense on both T1- and T2WI due to hemorrhagic and proteinaceous contents, with marked enhancement after gadolinium [50, 62, 63]. Angiography might be useful to assess intracranial vessel involvement and carotid artery infiltration before surgery [64].

Renal cysts and clear cell RCC occur in more than two-thirds of patients with VHL [50]. Renal cysts are usually bilateral and multiple, and their malignant potential depends on size and number [50, 65]. Cysts may be simple or complex (containing both cystic and solid components). US can help differentiate solid from cystic lesions; however, CT and MRI are preferred for further assessment. On CT, simple cysts appear as thin-walled lesions with fluid density with no or minimal enhancement. On MRI, they show homogeneous T1 hypointensity, T2 hyperintensity, and lack post-contrast enhancement [50, 65]. Complex cysts are precursors to RCC [65]. Solid RCCs are usually heterogeneous and demonstrate avid early enhancement followed by washout in the delayed phase [50]. On MRI, they are T1-hypointense, T2-hyperintense, and show marked enhancement. Cystic RCCs exhibit enhancing nodular components and/or thick nodular septa [50].

RCC is usually the most common cause of mortality in patients with VHL, and the presence of bilateral or multifocal RCC in individuals younger than 50 years should prompt VHL genetic testing [66]. VHL-associated RCCs

occur at a younger age than sporadic RCCs, with a mean age of 39 years [50].

Adrenal pheochromocytomas develop in 25-30% of patients with VHL [50]. The mean age of onset is 27 years and in 50% of cases they are bilateral [67]. Extra-adrenal location along the sympathetic chain in the abdomen, thorax, or head and neck have been seen in 15% of VHL cases [50, 65]. On CT, pheochromocytomas appear as solid or complex cystic masses with areas of necrosis and hemorrhage, calcifications, and marked enhancement [65]. However, CT enhancement characteristics may not distinguish them from other lesions that may show similar enhancement (adenomas, or hypervascular adrenal metastases) [68]. On MRI, they typically show iso- or hypointensity relative to the liver on T1WI and on T2WI they appear as a 'light-bulb' bright lesion comparable to the signal intensity of cerebrospinal fluid [68, 69]. ^{123}I-metaiodobenzylguanidine (MIBG) scintigraphy may be useful in tumor localization, although PET/CT offers higher sensitivity for detecting metastatic disease [70, 71]. The diagnosis of pheochromocytoma is confirmed on biochemical tests (serum and urinary catecholamines) [65].

Pancreatic manifestations in patients with VHL include cysts, serous cystoadenomas, and pancreatic neuroendocrine tumors (NETs). Pancreatic cysts are usually multiple, asymptomatic, and may represent the only manifestation at the time of initial diagnosis in up to 12% of patients [72]. On CT, they appear as hypoattenuating lesions with fluid attenuation and

without enhancement [50]. Serous cystoadenomas present as multilobulated cystic masses with a characteristic grape appearance on CT. An enhancing central scar with stellate calcification may be seen in 20% of cases [50]. On MRI, the central scar may appear hypointense on both T1 and T2WI with delayed enhancement. Pancreatic NETs are usually hypo- to isointense on CT and exhibit marked early arterial enhancement, sometimes with necrotic areas and heterogeneous enhancement in larger lesions [65]. Tumors smaller than 3 cm are usually solid and homogeneous. On MRI, they appear T1-hypointense and T2-hyperintense with avid arterial enhancement with washout on delayed phase images [50].

5. PTEN Hamartoma Tumor Syndrome – Cowden Syndrome

Cowden Syndrome (CS) is a rare cancer predisposition syndrome caused by autosomal dominant mutations in the PTEN tumor suppressor gene [73]. It is part of the PTEN hamartoma tumor syndrome (PHTS) family, which predisposes affected individuals to the development of hamartomas and an increased risk of benign and malignant tumors, particularly of the thyroid, breast, kidney, colon, and endometrium [73, 74]. Mucocutaneous lesions, observed in nearly all patients, are usually the earliest clinical manifestation and include papules, papillomas, trichilemmomas, and acral keratoses [75]. Other non-typical cutaneous lesions include angiomas, lipomas, neurinomas, xanthomas, melanomas, squamous cell carcinoma, and basal cell carcinoma

[73, 75]. In addition to cancer susceptibility and dermatologic findings, PHTS features include Lhermitte-Duclos disease, macrocephaly, vascular anomalies, and autism spectrum disorder [76-78]. Intracranial meningiomas have also been reported in the setting of CS, although this association remains unconfirmed [79, 80]. The National Comprehensive Cancer Network diagnostic criteria (Table 2) are currently used for diagnosing CS in individuals older than 18 years [76]. Bannayan-Riley-Ruvalcaba syndrome (BRRS) is considered a phenotypic form of CS in children and is characterized by macrocephaly, intestinal hamartomatous polyposis, lipomas, and pigmented macules of the glans penis [76, 77].

Lhermitte-Duclos Disease (LDD) is a benign dysplastic gangliocytoma of the cerebellum, usually diagnosed at approximately 20-30 years of age [76]. It usually affects a single cerebellar hemisphere, with a slight right-side predilection; the vermis may also be affected [81]. Patients typically present with ataxia, nystagmus, and increased intracranial pressure [82]. On MRI, LDD appears as a hyperintense T2/FLAIR cerebellar lesion with widening of the cerebellar folia, producing the characteristic “tigroid” appearance [83]. In children, however, diagnosis may be challenging because the typical “tiger stripe” pattern may be absent [84] and childhood-onset LDD is less frequently associated with PTEN mutations [76]. Although LDD is usually described as a non-enhancing, linear or dot-like enhancement, as well as curvilinear enhancement secondary to small draining veins, has been reported [85-88]. MRI is also valuable for

evaluating mass effect in the posterior fossa caused by LDD, and secondary obstructive hydrocephalus and cerebellar tonsillar herniation [89, 90]. Downward herniation of the cerebellar tonsils has been described in several cases and it is important to differentiate whether it is acquired or developmental, as it may also occur in the absence of LDD [85].

Vascular malformations, including arteriovenous malformations and hemangiomas, are frequently reported in BRRS and CS patients and are a minor criterion for the diagnosis of PHTS [76]. They present as multifocal, intramuscular, or intracranial developmental abnormalities [83] (Figure 6).

Macrocephaly in PHTS is typically due to generalized megalencephaly, characterized by brain overgrowth due to increased number or size of neurons and glial cells. In most patients, it is symmetrical, although cases with hemimegalencephaly have also been described [82, 91]. Brain MRI should also be assessed for other cortical malformations, including focal cortical dysplasia, polymicrogyria, and periventricular nodular heterotopia, all reported in children with PTEN mutation [92-94].

Breast cancer is the most common tumor in patients with CS. On MRI, breast lesions typically demonstrate enhancement on post-contrast images, often with irregular margins and suspicious washout or plateau enhancement kinetics, however, they do not demonstrate specific features that differentiate them from sporadic cases [83].

Thyroid carcinoma is the second most common cancer in patients with CS and patients have a risk of 3-10% of developing it [83]. Thyroid benign lesions are also very frequent starting in childhood and include nodular goiter, single or multiple adenomas, autoimmune thyroiditis [82]. US is the initial preferred imaging modality and helps differentiating benign from malignant lesions. Typically, solid hypoechoic nodules with irregular margins that lack a hypoechoic halo surrounding the nodule and internal vascularity with possible microcalcifications are suggestive features of malignant nodules. There are no imaging differences between CS-associated thyroid cancer and those in the general population [83].

Table 2. Clinical Diagnostic Criteria for Cowden Syndrome

Major criteria	Minor criteria
1. Breast cancer	1. Autism spectrum disorder
2. Endometrial cancer	2. Colorectal cancer
3. Follicular carcinoma of the thyroid gland	3. Esophageal glycogenic acanthosis (≥3)
4. Gastrointestinal hamartomas (including ganglioneuromas, but excluding hyperplastic polyps; ≥3)	4. Lipoma (≥3)
5. Adult-onset Lhermitte-Duclos disease	5. Intellectual disability (IQ ≤75)

6. Macrocephaly (>97th percentile: 58 cm in women and 60 cm in men)	6. Renal cell carcinoma
7. Macular pigmentation of the glans penis	7. Testicular lipomatosis
8. Multiple mucocutaneous lesions (any of the following): - Acral keratoses (≥3, palmoplantar keratotic pits and/or acral hyperkeratotic papules) - Multiple trichilemmomas (≥3, at least one biopsy proven): - Mucocutaneous neuroma (≥3)	8. Thyroid cancer (papillary carcinoma or follicular variant of papillary)
	9. Thyroid structural lesions (adenoma, adenomatous goiter, etc.)
	10. Vascular anomalies (e.g., multiple developmental venous anomalies)

6. Beckwith-Wiedemann Syndrome (BWS)

Beckwith-Wiedemann Syndrome is a rare multisystem overgrowth disorder caused by genetic and epigenetic defects affecting the chromosome 11p15.5 region [95, 96]. This locus contains several imprinted genes, including CDKN1C and IGF2, which play key roles in regulating fetal growth [95, 96]. BWS is typically diagnosed in the neonatal period or early childhood and is clinically characterized by macroglossia, macrosomia, abdominal wall

defects, hemihyperplasia, hemimegalencephaly, and severe neonatal hypoglycemia (Figure 7) [95]. Additional features include exophthalmos, hypertelorism, nystagmus, infraorbital creases, facial nevus flammeus, midfacial hypoplasia, full lower face with a prominent mandible, anterior earlobe creases and posterior helical pits [96] (Table 3).

Tumor risk is higher during the first decade of life, with a marked predisposition to embryonal tumors, particularly Wilms tumor (WT) and hepatoblastoma [97]. Less frequently, rhabdomyosarcoma, adrenocortical carcinoma, and neuroblastoma have also been reported [97]. An increased tumor risk has been observed in patients presenting with hemihyperplasia or nephromegaly [98].

WT is the most frequently reported tumor in patients with BWS, occurring in approximately 1-8% of affected individuals [99]. Compared to sporadic cases, BWS-associated WTs tend to present earlier (typically before 2 years of age), are often bilateral or multifocal, and frequently coexist with nephrogenic rests (NRs) - persistent embryonal tissue representing WT precursors [100, 101]. Abdominal US is usually the initial imaging modality in suspected WT, and prenatal US, particularly in the presence of omphalocele, may enable early diagnosis of BWS [102, 103]. On US, WTs typically appear as intrarenal masses with a pseudocapsule, often containing large hypoechoic areas reflecting central necrosis, hemorrhage and cyst formation [104]. On MRI, the ‘claw sign’ – in which the normal renal parenchyma stretches and wraps around the mass- is indicative of WT

[105, 106]. These tumors are generally hypointense on T1WI and demonstrate variable to high signal intensity on T2WI with non-cystic components typically showing diffusion restriction. In contrast to neuroblastoma, vessels are displaced rather than encased, and vascular invasion occurs in approximately 5-10% of cases [104, 105]. NRs are observed in up to 70-80% of patients with BWS-associated WT and are usually located at the periphery of the renal cortex (perilobar NRs) [100, 107]. Post-contrast T1WI can help differentiate NRs or nephroblastomatosis (multiple or diffusely distributed NRs) from WTs, as in contrast to WTs, these lesions show little or no enhancement following contrast administration [106].

Hepatoblastomas are large, well circumcised neoplasms and occur in approximately 8-14% of patients with BWS [108]. On US, they are hyperechoic relative to the adjacent liver, though echogenicity may vary depending on the histologic type [108, 109]. Mixed tumors appear heterogeneous with calcifications causing echogenic shadowing, and anechoic foci reflecting hemorrhage and necrosis; hypoechoic septa may also be present. On CT they are hypoattenuating compared to normal liver parenchyma and demonstrate mild post-contrast enhancement. On MRI, lesions are usually hypointense on T1WI and hyperintense on T2WI, with diffusion restriction in solid components of mixed tumors [108, 109].

Table 3. Clinical Features of Beckwith–Wiedemann Syndrome

Major Findings:
• Abdominal wall defect: omphalocele or umbilical hernia • Macroglossia • Macrosomia* (defined as height and weight >97th percentile) • Anterior ear lobe creases and/or posterior helical pits (bilateral or unilateral) • Visceromegaly of intra-abdominal organ • Embryonal tumor in childhood • Hemihyperplasia • Cytomegaly of adrenal fetal cortex, usually diffuse and bilateral • Renal abnormalities, including medullary dysplasia and later development of medullary sponge kidney • Positive family history of BWS • Cleft palate
Minor findings
• Polyhydramnios, enlarged placenta and/or thickened umbilical cord, premature birth • Neonatal hypoglycemia • Nevus flammeus • Cardiomegaly/structural cardiac anomalies/cardiomyopathy • Characteristic facies

- Diastasis recti
- Advanced bone age

.

7. Multiple endocrine Neoplasia

Multiple endocrine neoplasia (MEN) is a group of autosomal dominant disorders that predispose affected individuals to the development of benign and malignant endocrine and neuroendocrine tumors (Table 4) [110]. MEN1 is caused by mutations in the MEN1 tumor suppressor gene and is characterized by tumors of the parathyroid glands (95%), pancreas (40%), and pituitary gland (30%) [110, 111]. Additional manifestations include angiofibromas, collagenomas, adrenal cortical tumors, and facial ependymomas [111]. MEN 2 includes MEN2A, MEN2B, and familial medullary thyroid carcinoma (FMTC) and results from mutations of the RET proto-oncogene [3]. The hallmark tumors of MEN2 include medullary thyroid carcinoma (MTC), adrenal pheochromocytomas, and parathyroid tumors.

Parathyroid adenomas are the most common tumors and usually the presenting feature of MEN1 [110, 112]. Hyperparathyroidism occurs in more than 90% of patients, typically between 20-25 years of age [111]. In contrast to sporadic cases - where a solitary adenoma is present in 90% of patients – individuals with MEN1 demonstrate asymmetric multiple glands

disease [112]. MEN2A is also associated with multiglandular involvement, but it has usually a later onset and occurs in the setting of concomitant MTC [112, 113].

On US, parathyroid adenomas appear as well defined, oval hypoechoic masses posterior to the thyroid gland. Large adenomas may appear multilobulated and contain echogenic foci [112, 114]. Color and power Doppler demonstrate a prominent feeding artery that courses along the periphery before entering the gland, producing a characteristic arc or rim of vascularity [114]. Focal asymmetric hypervascularities of the overlying thyroid gland may further assist localization of the underlying adenoma [114].

CT provides no additional information, but it is helpful for identifying abnormal ectopic glands within the mediastinum or behind the trachea.

On single-photon emission computed tomography sestamibi imaging, adenomas show asymmetric focal radiotracer uptake with retention on delayed imaging, distinguishing them from normal tissue [110, 114].

Parathyroid adenomas are typically hypointense on T1WI and hyperintense on T2WI, though MRI is not usually used for diagnosis [112].

Anterior pituitary adenomas occur in approximately 30% of MEN1 patients [112]. Up to 60% of the hormone-secreting tumors are prolactinomas, followed by growth hormone-secreting tumors (<25%), and, rarely, adrenocortical hormone- or thyroid stimulating hormone- secreting tumors [115]. Non-functioning adenomas account for about 5% [110].

Small field view MRI with ≤ 3 mm slice-thickness pre- and post-contrast T1WI of the sella is the imaging modality of choice [112]. Adenomas typically appear hypointense relative to the normal pituitary tissue on both pre- and post-contrast T1WI (Figure 8). Microadenomas (<10mm) may not always be visualized on imaging; however, secondary signs – such as focal convexity of the superior pituitary gland, deviation of the pituitary stalk or lowering/erosion of the sellar floor - may suggest the diagnosis. Dynamic contrast-enhanced MRI may increase the differences in enhancement between microadenomas and the normal pituitary tissue reviewing early and delayed phase imaging [116]. Microadenomas typically show less contrast enhancement compared to the normal pituitary gland tissue on the early arterial phases with persistent contrast enhancement on the late phase images. Macroadenomas (>10mm) are usually isointense to gray matter on T1WI, however, attenuation and signal characteristics vary significantly depending on tumor components such as hemorrhage, cystic transformation, or necrosis [115]. Mass effect on adjacent structures is common [110].

Pancreatic NETs occur in approximately 80% of MEN1 patients and may be functioning or nonfunctioning [110]. Gastrinomas are the most common (60%), followed by insulinomas (30%); glucagonomas VIPomas, and somatostatinomas represent less than 5% [113, 117]. Transabdominal US has low sensitivity for detecting pancreatic NETs. Endoscopic US is much more sensitive but invasive and limited to

specialized centers [112]. Intraoperative US is highly effective, typically showing solid hypoechoic masses with occasional hypo- to anechoic cystic foci and calcified components [115].

CT is the most widely used modality for localization [112]. NETs appear as small (<2cm), often multiple, arterial-phase–enhancing lesions, isodense to the pancreas on non-contrast images. CT is also useful for evaluating local invasion or liver metastases [110, 112].

MRI offers a superior sensitivity for small lesions. NETs are typically T1-hypointense and T2-hyperintense, although T2 signal may be reduced in highly collagenous tumors [110, 112]. Liver metastases often display early arterial peripheral ring enhancement [112, 115].

Somatostatin receptor imaging with ^{111}In-octreotide helps detect NETs with somatostatin receptors. ^{18}F-FDG PET may identify aggressive NETs that typically lack somatostatin receptor expression, but demonstrate hypermetabolic activity [112].

Adrenal cortical adenomas occur in up to 40% of MEN1 patients and are usually nonfunctioning [118]. CT or MRI are diagnostic. Up to 80% are lipid-rich, showing very low CT attenuation (<10 HU), and signal dropout on opposed-phase T1W gradient recalled echo images [119]. Adrenal cortical carcinomas are very rare, but present as large heterogeneous masses with central necrosis, hemorrhage and calcification, with potential local invasion and distant metastases [110].

MTC is multicentric, bilateral and occurs in nearly all MEN2 patients. It is aggressive and may metastasize to the liver, lungs, bones and brain. Serum calcitonin and carcinoembryonic antigen levels are usually elevated. On US, CT, and MRI, MTC appears as a solid mass often containing calcifications. Whole-body radionuclide imaging with ^{123}I-MIBG, pentavalent ^{99m}Tc-dimer-captosuccinic acid, and somatostatin analogues such as ^{111}I-octreotide allows accurate staging [112].

Pheochromocytomas occur in up to 50% of MEN2 patients and are bilateral in most cases [120]. Biochemical screening with urinary metanephrines and imaging is essential before thyroid surgery to reduce perioperative morbidity and mortality [113].

On CT, lesions typically have attenuation >10 HU and show avid enhancement after contrast administration [121]. CT has near-100% sensitivity, but MRI is preferred due to lack of radiation and the characteristic “light-bulb bright” T2 hyperintensity [110].

^{18}F-DOPA PET/CT is recommended as first-line imaging for patients with inherited forms of pheochromocytoma, whereas ^{123}I-MIBG may be considered first line in sporadic cases [122].

Table 4. Clinical Features of MEN Syndromes

MEN1	MEN2A	MEN2B	FMTC

Parathyroid tumors	Medullary thyroid carcinoma	Medullary thyroid carcinoma	Familial medullary thyroid carcinoma
Pancreatic islet cell tumors	Pheochromocytoma	Pheochromocytoma	
Pituitary tumors	Parathyroid tumor	Associated abnormalities: - Mucosal neuromas - Marfanoid habitus - Multiple ganglioneuromas	
Other tumors: - Angiofibromas - Collagenomas - Adrenal cortical tumors - Carcinoid tumors			

8. Conclusion

Imaging plays a central role in the evaluation of patients with CPSs. Given the wide spectrum of benign and malignant tumors associated with these disorders, imaging assessment—together with genetic testing—is essential for both diagnosis and surveillance. Familiarity with characteristic imaging patterns enables early tumor detection and supports timely clinical management, ultimately improving outcomes for individuals with suspected or confirmed CPS.

List of abbreviations

BRRS: Bannayan-Riley-Ruvalcaba syndrome; BWS: Beckwith-Wiedemann Syndrome; CNS: central nervous system; CPS: cancer predisposition syndrome; CS: Cowden syndrome; FASI: focal areas of signal intensity; FMTC: familial medullary thyroid carcinoma; IAC: internal auditory canal; LDD: Lhermitte-Duclos disease; MEN: multiple endocrine neoplasia; MIBG: metaiodobenzylguanidine; MTC: medullary thyroid carcinoma; NETs: neuroendocrine tumors; NF1: neurofibromatosis type 1; NF2: neurofibromatosis type 2; NRs: nephrogenic rests; OPG: optic pathway glioma; PHTS: PTEN hamartoma tumor syndrome; RCC: renal cell carcinoma; US: ultrasound; VHL: Von Hippel-Lindau; WI: weighted image; WT: Wilms tumor

Declarations

Ethics approval and consent to participate

Not applicable.

Consent for publication

All authors agreed with the content of this manuscript and approved the submitted version.

Data availability

No datasets were generated or analyzed during the current study.

Competing interests

The authors declare no competing interests.

Funding

No funding.

Author contributions

LM: conceptualization, literature search, writing-original draft, figure editing, writing-review and editing. HBT: writing-review and editing, figure preparation. DM: literature search, writing-original draft. ML, ND: writing-review and editing. TAGMH: conceptualization, writing-review and editing, figure editing. All authors contributed and approved the submitted version.

References

1. Knapke S, Zelley K, Nichols KE, Kohlmann W, Schiffman JD: **Identification, management, and evaluation of children with cancer-predisposition syndromes**. *Am Soc Clin Oncol Educ Book* 2012:576-584.
2. Mertiri L, Desai N, Lequin M, Mertiri D, Tran HB, Alves C, Chiocchi M, Huisman T, D'Arco F: **Cancer Predisposition Syndromes With Involvement of the Head and Neck Regions in Children: An Imaging Guide**. *J Neuroimaging* 2025, **35**(5):e70092.
3. Monsalve J, Kapur J, Malkin D, Babyn PS: **Imaging of cancer predisposition syndromes in children**. *Radiographics* 2011, **31**(1):263-280.
4. Ahlawat S, Blakeley JO, Langmead S, Belzberg AJ, Fayad LM: **Current status and recommendations for imaging in neurofibromatosis type 1, neurofibromatosis type 2, and schwannomatosis**. *Skeletal Radiol* 2020, **49**(2):199-219.
5. Rodriguez D, Young Poussaint T: **Neuroimaging findings in neurofibromatosis type 1 and 2**. *Neuroimaging Clin N Am* 2004, **14**(2):149-170, vii.
6. Kresak JL, Walsh M: **Neurofibromatosis: A Review of NF1, NF2, and Schwannomatosis**. *J Pediatr Genet* 2016, **5**(2):98-104.
7. Ozarslan B, Russo T, Argenziano G, Santoro C, Piccolo V: **Cutaneous Findings in Neurofibromatosis Type 1**. *Cancers (Basel)* 2021, **13**(3).
8. Zulfiqar M, Lin M, Ratkowski K, Gagnon M-H, Menias C, Siegel CL: **Imaging Features of Neurofibromatosis Type 1 in the Abdomen and Pelvis**. *American Journal of Roentgenology* 2021, **216**(1):241-251.
9. Wang MX, Dillman JR, Guccione J, Habiba A, Maher M, Kamel S, Panse PM, Jensen CT, Elsayes KM: **Neurofibromatosis from Head to Toe: What the Radiologist Needs to Know**. *Radiographics* 2022, **42**(4):1123-1144.
10. Di Pietro S, Reali L, Tona E, Belfiore G, Praticò AD, Ruggieri M, David E, Foti PV, Santonocito OG, Basile A *et al*: **Magnetic Resonance Imaging of Central Nervous System Manifestations of Type 1 Neurofibromatosis: Pictorial Review and Retrospective Study of Their Frequency in a Cohort of Patients**. In: *Journal of Clinical Medicine.* vol. 13; 2024.
11. **Friedman JM. Neurofibromatosis 1. 1998 Oct 2 [Updated 2022 Apr 21]. In: Adam MP, Feldman J, Mirzaa GM, et al., editors. GeneReviews® [Internet]. Seattle (WA): University of Washington, Seattle; 1993-2025. Available from: https://www.ncbi.nlm.nih.gov/books/NBK1109/**.
12. Mentzel HJ, Seidel J, Fitzek C, Eichhorn A, Vogt S, Reichenbach JR, Zintl F, Kaiser WA: **Pediatric brain MRI in neurofibromatosis type I**. *Eur Radiol* 2005, **15**(4):814-822.
13. Prada CE, Rangwala FA, Martin LJ, Lovell AM, Saal HM, Schorry EK, Hopkin RJ: **Pediatric plexiform neurofibromas: impact on morbidity and mortality in neurofibromatosis type 1**. *J Pediatr* 2012, **160**(3):461-467.
14. Evans DG, Baser ME, McGaughran J, Sharif S, Howard E, Moran A: **Malignant peripheral nerve sheath tumours in neurofibromatosis 1**. *J Med Genet* 2002, **39**(5):311-314.
15. Hirbe AC, Dehner CA, Dombi E, Eulo V, Gross AM, Sundby T, Lazar AJ, Widemann BC: **Contemporary Approach to Neurofibromatosis Type 1–**

Associated Malignant Peripheral Nerve Sheath Tumors. *American Society of Clinical Oncology Educational Book* 2024, **44**(3):e432242.
16. Carton C, Evans DG, Blanco I, Friedrich RE, Ferner RE, Farschtschi S, Salvador H, Azizi AA, Mautner V, Röhl C *et al*: **ERN GENTURIS tumour surveillance guidelines for individuals with neurofibromatosis type 1**. *EClinicalMedicine* 2023, **56**:101818.
17. Russo C, Russo C, Cascone D, Mazio F, Santoro C, Covelli EM, Cinalli G: **Non-Oncological Neuroradiological Manifestations in NF1 and Their Clinical Implications**. *Cancers (Basel)* 2021, **13**(8).
18. Toro G, Santoro C, Ambrosio D, Landi G, Scilipoti M, Moretti A, Paoletta M, Liguori S, Schiavone Panni A, Picariello S *et al*: **Natural History of Scoliosis in Children with NF1: An Observation Study**. *Healthcare (Basel)* 2021, **9**(7).
19. DiPaolo DP, Zimmerman RA, Rorke LB, Zackai EH, Bilaniuk LT, Yachnis AT: **Neurofibromatosis type 1: pathologic substrate of high-signal-intensity foci in the brain**. *Radiology* 1995, **195**(3):721-724.
20. Griffiths PD, Blaser S, Mukonoweshuro W, Armstrong D, Milo-Mason G, Cheung S: **Neurofibromatosis bright objects in children with neurofibromatosis type 1: a proliferative potential?** *Pediatrics* 1999, **104**(4):e49.
21. Piscitelli O, Digilio MC, Capolino R, Longo D, Di Ciommo V: **Neurofibromatosis type 1 and cerebellar T2-hyperintensities: the relationship to cognitive functioning**. *Dev Med Child Neurol* 2012, **54**(1):49-51.
22. Feldmann R, Schuierer G, Wessel A, Neveling N, Weglage J: **Development of MRI T2 hyperintensities and cognitive functioning in patients with neurofibromatosis type 1**. *Acta Paediatr* 2010, **99**(11):1657-1660.
23. Hyman SL, Gill DS, Shores EA, Steinberg A, North KN: **T2 hyperintensities in children with neurofibromatosis type 1 and their relationship to cognitive functioning**. *J Neurol Neurosurg Psychiatry* 2007, **78**(10):1088-1091.
24. Listernick R, Ferner RE, Liu GT, Gutmann DH: **Optic pathway gliomas in neurofibromatosis-1: controversies and recommendations**. *Ann Neurol* 2007, **61**(3):189-198.
25. Listernick R, Charrow J, Greenwald M, Mets M: **Natural history of optic pathway tumors in children with neurofibromatosis type 1: a longitudinal study**. *J Pediatr* 1994, **125**(1):63-66.
26. Parsa CF, Hoyt CS, Lesser RL, Weinstein JM, Strother CM, Muci-Mendoza R, Ramella M, Manor RS, Fletcher WA, Repka MX *et al*: **Spontaneous regression of optic gliomas: thirteen cases documented by serial neuroimaging**. *Arch Ophthalmol* 2001, **119**(4):516-529.
27. D'Arco F, Mertiri L, de Graaf P, De Foer B, Popovič KS, Argyropoulou MI, Mankad K, Brisse HJ, Juliano A, Severino M *et al*: **Guidelines for magnetic resonance imaging in pediatric head and neck pathologies: a multicentre international consensus paper**. *Neuroradiology* 2022, **64**(6):1081-1100.
28. Ullrich NJ, Raja AI, Irons MB, Kieran MW, Goumnerova L: **Brainstem lesions in neurofibromatosis type 1**. *Neurosurgery* 2007, **61**(4):762-766; discussion 766-767.

29. Mahdi J, Shah AC, Sato A, Morris SM, McKinstry RC, Listernick R, Packer RJ, Fisher MJ, Gutmann DH: **A multi-institutional study of brainstem gliomas in children with neurofibromatosis type 1**. *Neurology* 2017, **88**(16):1584-1589.
30. Coy S, Rashid R, Stemmer-Rachamimov A, Santagata S: **An update on the CNS manifestations of neurofibromatosis type 2**. *Acta Neuropathol* 2020, **139**(4):643-665.
31. Lloyd SK, Evans DG: **Neurofibromatosis type 2 (NF2): diagnosis and management**. *Handb Clin Neurol* 2013, **115**:957-967.
32. Bosch MM, Boltshauser E, Harpes P, Landau K: **Ophthalmologic findings and long-term course in patients with neurofibromatosis type 2**. *Am J Ophthalmol* 2006, **141**(6):1068-1077.
33. Rai P, Bathla G, Soni N, Desai A, Rao D, Vibhute P, Agarwal A: **Classification of schwannomas and the new naming convention for "neurofibromatosis-2": Genetic updates and international consensus recommendation**. *Neuroradiol J* 2025, **38**(5):533-542.
34. Ruggieri M, Iannetti P, Polizzi A, La Mantia I, Spalice A, Giliberto O, Platania N, Gabriele AL, Albanese V, Pavone L: **Earliest clinical manifestations and natural history of neurofibromatosis type 2 (NF2) in childhood: a study of 24 patients**. *Neuropediatrics* 2005, **36**(1):21-34.
35. Baser ME, Mautner VF, Parry DM, Evans DG: **Methodological issues in longitudinal studies: vestibular schwannoma growth rates in neurofibromatosis 2**. *J Med Genet* 2005, **42**(12):903-906.
36. Baser ME, Makariou EV, Parry DM: **Predictors of vestibular schwannoma growth in patients with neurofibromatosis Type 2**. *J Neurosurg* 2002, **96**(2):217-222.
37. Lin EP, Crane BT: **The Management and Imaging of Vestibular Schwannomas**. *AJNR Am J Neuroradiol* 2017, **38**(11):2034-2043.
38. Zhao F, Wang B, Yang Z, Zhou Q, Li P, Wang X, Zhang J, Zhang J, Liu P: **Surgical treatment of large vestibular schwannomas in patients with neurofibromatosis type 2: outcomes on facial nerve function and hearing preservation**. *J Neurooncol* 2018, **138**(2):417-424.
39. Fisher LM, Doherty JK, Lev MH, Slattery WH, 3rd: **Distribution of nonvestibular cranial nerve schwannomas in neurofibromatosis 2**. *Otol Neurotol* 2007, **28**(8):1083-1090.
40. Plana-Pla A, García B, Munera-Campos M, Catasus N, Serra Arenas E, Blanco I, Castellanos Perez E, Bielsa I, HUGTiP-ICO-IGTP NMC: **Skin lesions in neurofibromatosis type 2: diagnostic and prognostic significance of cutaneous (plexiform) schwannomas**. *Journal of the European Academy of Dermatology and Venereology* 2022, **36**(9):1632-1640.
41. Berg JC, Scheithauer BW, Spinner RJ, Allen CM, Koutlas IG: **Plexiform schwannoma: a clinicopathologic overview with emphasis on the head and neck region**. *Hum Pathol* 2008, **39**(5):633-640.
42. Ko JY, Kim JE, Kim YH, Ro YS: **Cutaneous plexiform schwannomas in a patient with neurofibromatosis type 2**. *Ann Dermatol* 2009, **21**(4):402-405.
43. Kabashi S, Ugurel MS, Dedushi K, Mucaj S: **The Role of Magnetic Resonance Imaging (MRI) in Diagnostics of Acoustic Schwannoma**. *Acta Inform Med* 2020, **28**(4):287-291.

44. Luo M, Wang W, Zeng Q, Luo Y, Yang H, Yang X: **Tuberculous meningitis diagnosis and treatment in adults: A series of 189 suspected cases**. *Exp Ther Med* 2018, **16**(3):2770-2776.
45. Kim WY, Kim IO, Kim S, Cheon JE, Yeon M: **Meningioangiomatosis: MR imaging and pathological correlation in two cases**. *Pediatr Radiol* 2002, **32**(2):96-98.
46. Kim HJ, Paul F, Lana-Peixoto MA, Tenembaum S, Asgari N, Palace J, Klawiter EC, Sato DK, de Seze J, Wuerfel J *et al*: **MRI characteristics of neuromyelitis optica spectrum disorder: an international update**. *Neurology* 2015, **84**(11):1165-1173.
47. Plotkin SR, O'Donnell CC, Curry WT, Bove CM, MacCollin M, Nunes FP: **Spinal ependymomas in neurofibromatosis Type 2: a retrospective analysis of 55 patients**. *J Neurosurg Spine* 2011, **14**(4):543-547.
48. Louise MBM, Smerdel M, Borgwadt L, Beck Nielsen SS, Madsen MG, Møller HU, Kiilgaard JF, Friis-Hansen L, Harbud V, Cortnum S *et al*: **von Hippel-Lindau disease: Updated guideline for diagnosis and surveillance**. *Eur J Med Genet* 2022, **65**(8):104538.
49. Klingler JH, Gläsker S, Bausch B, Urbach H, Krauss T, Jilg CA, Steiert C, Puzik A, Neumann-Haefelin E, Kotsis F *et al*: **Hemangioblastoma and von Hippel-Lindau disease: genetic background, spectrum of disease, and neurosurgical treatment**. *Childs Nerv Syst* 2020, **36**(10):2537-2552.
50. Ganeshan D, Menias CO, Pickhardt PJ, Sandrasegaran K, Lubner MG, Ramalingam P, Bhalla S: **Tumors in von Hippel–Lindau Syndrome: From Head to Toe—Comprehensive State-of-the-Art Review**. *RadioGraphics* 2018, **38**(3):849-866.
51. Wanebo JE, Lonser RR, Glenn GM, Oldfield EH: **The natural history of hemangioblastomas of the central nervous system in patients with von Hippel-Lindau disease**. *J Neurosurg* 2003, **98**(1):82-94.
52. Rumboldt Z, Matheus MG: **Hemangioblastoma**. In: *Brain Imaging with MRI and CT: An Image Pattern Approach.* Edited by Rumboldt Z, Castillo M, Huang B, Rossi A. Cambridge: Cambridge University Press; 2012: 361-362.
53. Setyawan NH, Hartanto RA, Malueka RG, Dwianingsih EK, Dharma DP: **Dual manifestations: spinal and cerebellar hemangioblastomas indicative of von Hippel-Lindau syndrome**. *Radiology Case Reports* 2024, **19**(11):5000-5006.
54. Pietrzak N, Jankowska K, Rosiak O, Konopka W: **New Prospects on Neuroimaging in Von Hippel Lindau Disease—A Narrative Review**. In: *Diagnostics.* vol. 14; 2024.
55. Lonser RR, Butman JA, Huntoon K, Asthagiri AR, Wu T, Bakhtian KD, Chew EY, Zhuang Z, Linehan WM, Oldfield EH: **Prospective natural history study of central nervous system hemangioblastomas in von Hippel-Lindau disease**. *J Neurosurg* 2014, **120**(5):1055-1062.
56. She DJ, Xing Z, Zeng Z, Shang XY, Cao DR: **Differentiation of hemangioblastomas from pilocytic astrocytomas using 3-T magnetic resonance perfusion-weighted imaging and MR spectroscopy**. *Neuroradiology* 2015, **57**(3):275-281.
57. AlRayahi J, Zapotocky M, Ramaswamy V, Hanagandi P, Branson H, Mubarak W, Raybaud C, Laughlin S: **Pediatric Brain Tumor Genetics: What Radiologists Need to Know**. *RadioGraphics* 2018, **38**(7):2102-2122.

58. Chittiboina P, Lonser RR: **Von Hippel-Lindau disease**. *Handb Clin Neurol* 2015, **132**:139-156.
59. Dollfus Hln, Massin P, Taupin P, Nemeth C, Amara S, Giraud S, Béroud C, Dureau P, Gaudric A, Landais P *et al*: **Retinal Hemangioblastoma in von Hippel-Lindau Disease: A Clinical and Molecular Study**. *Investigative Ophthalmology & Visual Science* 2002, **43**(9):3067-3074.
60. Wong WT, Agrón E, Coleman HR, Tran T, Reed GF, Csaky K, Chew EY: **Clinical characterization of retinal capillary hemangioblastomas in a large population of patients with von Hippel-Lindau disease**. *Ophthalmology* 2008, **115**(1):181-188.
61. Tang X, Ji HM, Li WW, Ding ZX, Ye SL: **Imaging features of retinal hemangioblastoma: A case report**. *World J Clin Cases* 2023, **11**(3):692-699.
62. Patel NP, Wiggins RH, 3rd, Shelton C: **The radiologic diagnosis of endolymphatic sac tumors**. *Laryngoscope* 2006, **116**(1):40-46.
63. Mukherji SK, Albernaz VS, Lo WW, Gaffey MJ, Megerian CA, Feghali JG, Brook A, Lewin JS, Lanzieri CF, Talbot JM *et al*: **Papillary endolymphatic sac tumors: CT, MR imaging, and angiographic findings in 20 patients**. *Radiology* 1997, **202**(3):801-808.
64. Zanoletti E, Girasoli L, Borsetto D, Opocher G, Mazzoni A, Martini A: **Endolymphatic sac tumour in von Hippel-Lindau disease: management strategies**. *Acta Otorhinolaryngol Ital* 2017, **37**(5):423-429.
65. Taouli B, Ghouadni M, Corréas JM, Hammel P, Couvelard A, Richard S, Vilgrain V: **Spectrum of abdominal imaging findings in von Hippel-Lindau disease**. *AJR Am J Roentgenol* 2003, **181**(4):1049-1054.
66. Solomon D, Schwartz A: **Renal pathology in von Hippel-Lindau disease**. *Hum Pathol* 1988, **19**(9):1072-1079.
67. Aufforth RD, Ramakant P, Sadowski SM, Mehta A, Trebska-McGowan K, Nilubol N, Pacak K, Kebebew E: **Pheochromocytoma Screening Initiation and Frequency in von Hippel-Lindau Syndrome**. *J Clin Endocrinol Metab* 2015, **100**(12):4498-4504.
68. Schieda N, Alrashed A, Flood TA, Samji K, Shabana W, McInnes MD: **Comparison of Quantitative MRI and CT Washout Analysis for Differentiation of Adrenal Pheochromocytoma From Adrenal Adenoma**. *AJR Am J Roentgenol* 2016, **206**(6):1141-1148.
69. Neumann HP, Bender BU, Berger DP, Laubenberger J, Schultze-Seemann W, Wetterauer U, Ferstl FJ, Herbst EW, Schwarzkopf G, Hes FJ *et al*: **Prevalence, morphology and biology of renal cell carcinoma in von Hippel-Lindau disease compared to sporadic renal cell carcinoma**. *J Urol* 1998, **160**(4):1248-1254.
70. Janssen I, Chen CC, Millo CM, Ling A, Taieb D, Lin FI, Adams KT, Wolf KI, Herscovitch P, Fojo AT *et al*: **PET/CT comparing (68)Ga-DOTATATE and other radiopharmaceuticals and in comparison with CT/MRI for the localization of sporadic metastatic pheochromocytoma and paraganglioma**. *Eur J Nucl Med Mol Imaging* 2016, **43**(10):1784-1791.
71. Tan TH, Hussein Z, Saad FF, Shuaib IL: **Diagnostic Performance of (68)Ga-DOTATATE PET/CT, (18)F-FDG PET/CT and (131)I-MIBG Scintigraphy in Mapping Metastatic Pheochromocytoma and Paraganglioma**. *Nucl Med Mol Imaging* 2015, **49**(2):143-151.

72. Charlesworth M, Verbeke CS, Falk GA, Walsh M, Smith AM, Morris-Stiff G: **Pancreatic lesions in von Hippel-Lindau disease? A systematic review and meta-synthesis of the literature**. *J Gastrointest Surg* 2012, **16**(7):1422-1428.
73. Tan MH, Mester JL, Ngeow J, Rybicki LA, Orloff MS, Eng C: **Lifetime cancer risks in individuals with germline PTEN mutations**. *Clin Cancer Res* 2012, **18**(2):400-407.
74. Yehia L ECPHTSNUAIAM, Feldman J, Mirzaa GM, et al., editors. GeneReviews® [Internet]. Seattle (WA): University of Washington, Seattle; 1993-2025. Available from: https://www.ncbi.nlm.nih.gov/books/NBK1488/.
75. Masmoudi A, Chermi ZM, Marrekchi S, Raida BS, Boudaya S, Mseddi M, Jalel MT, Turki H: **Cowden syndrome**. *J Dermatol Case Rep* 2011, **5**(1):8-13.
76. Pilarski R: **PTEN Hamartoma Tumor Syndrome: A Clinical Overview**. *Cancers (Basel)* 2019, **11**(6).
77. Zelenova E, Belysheva T, Sharapova E, Barinova I, Fedorova A, Semenova V, Vishnevskaya Y, Kletskaya I, Mitrofanova A, Sofronov D *et al*: **Atypical Manifestations of Cowden Syndrome in Pediatric Patients**. *Diagnostics (Basel)* 2025, **15**(12).
78. Caroleo AM, Rotulo S, Agolini E, Macchiaiolo M, Boccuto L, Antonelli M, Colafati GS, Cacchione A, Megaro G, Carai A *et al*: **SHH medulloblastoma and very early onset of bowel polyps in a child with PTEN hamartoma tumor syndrome**. *Front Mol Neurosci* 2023, **16**:1228389.
79. Yakubov E, Ghoochani A, Buslei R, Buchfelder M, Eyüpoglu IY, Savaskan N: **Hidden association of Cowden syndrome, PTEN mutation and meningioma frequency**. *Oncoscience* 2016, **3**(5-6):149-155.
80. Dhamija R, Weindling SM, Porter AB, Hu LS, Wood CP, Hoxworth JM: **Neuroimaging abnormalities in patients with Cowden syndrome: Retrospective single-center study**. *Neurol Clin Pract* 2018, **8**(3):207-213.
81. Pereira VM, Geibprasert S, Krings T, Aurboonyawat T, Ozanne A, Toulgoat F, Pongpech S, Lasjaunias PL: **Pathomechanisms of symptomatic developmental venous anomalies**. *Stroke* 2008, **39**(12):3201-3215.
82. Macken WL, Tischkowitz M, Lachlan KL: **PTEN Hamartoma tumor syndrome in childhood: A review of the clinical literature**. *Am J Med Genet C Semin Med Genet* 2019, **181**(4):591-610.
83. Dragoo DD, Taher A, Wong VK, Elsaiey A, Consul N, Mahmoud HS, Mujtaba B, Stanietzky N, Elsayes KM: **PTEN Hamartoma Tumor Syndrome/Cowden Syndrome: Genomics, Oncogenesis, and Imaging Review for Associated Lesions and Malignancy**. *Cancers (Basel)* 2021, **13**(13).
84. Ma J, Jia G, Chen S, Jia W: **Clinical Perspective on Dysplastic Gangliocytoma of the Cerebellum (Lhermitte-Duclos Disease)**. *World Neurosurg* 2019, **122**:16-23.
85. Dhamija R, Wood CP, Porter AB, Hu LS, Weindling SM, Hoxworth JM: **Updated Imaging Features of Dysplastic Cerebellar Gangliocytoma**. *J Comput Assist Tomogr* 2019, **43**(2):277-281.
86. Awwad EE, Levy E, Martin DS, Merenda GO: **Atypical MR appearance of Lhermitte-Duclos disease with contrast enhancement**. *AJNR Am J Neuroradiol* 1995, **16**(8):1719-1720.
87. Chiofalo MG, Cappabianca P, Del Basso De Caro ML, Pezzullo L: **Lhermitte-Duclos disease**. *J Neurooncol* 2007, **82**(2):183-185.

88. Spaargaren L, Cras P, Bomhof MA, Lie ST, de Barsy AM, Croese PH, Teepen JL, Duwel VH, Van Goethem JW, Ozsarlak O *et al*: **Contrast enhancement in Lhermitte-Duclos disease of the cerebellum: correlation of imaging with neuropathology in two cases**. *Neuroradiology* 2003, **45**(6):381-385.
89. Dhamija R, Hoxworth JM: **Imaging of PTEN-related abnormalities in the central nervous system**. *Clin Imaging* 2020, **60**(2):180-185.
90. Yang MS, Kim CH, Cheong JH, Kim JM: **Lhermitte-Duclos disease presenting with hydrocephalus**. *Acta Neurochir Suppl* 2012, **113**:161-165.
91. Ghusayni R, Sachdev M, Gallentine W, Mikati MA, McDonald MT: **Hemimegalencephaly with Bannayan-Riley-Ruvalcaba syndrome**. *Epileptic Disord* 2018, **20**(1):30-34.
92. Elia M, Amato C, Bottitta M, Grillo L, Calabrese G, Esposito M, Carotenuto M: **An atypical patient with Cowden syndrome and PTEN gene mutation presenting with cortical malformation and focal epilepsy**. *Brain Dev* 2012, **34**(10):873-876.
93. Adachi T, Takigawa H, Nomura T, Watanabe Y, Kowa H: **Cowden Syndrome with a Novel PTEN Mutation Presenting with Partial Epilepsy Related to Focal Cortical Dysplasia**. *Intern Med* 2018, **57**(1):97-99.
94. Cheung KM, Lam CW, Chan YK, Siu WK, Yong L: **Atypical focal cortical dysplasia in a patient with Cowden syndrome**. *Hong Kong Med J* 2014, **20**(2):165-167.
95. Brioude F, Kalish JM, Mussa A, Foster AC, Bliek J, Ferrero GB, Boonen SE, Cole T, Baker R, Bertoletti M *et al*: **Clinical and molecular diagnosis, screening and management of Beckwith–Wiedemann syndrome: an international consensus statement**. *Nature Reviews Endocrinology* 2018, **14**(4):229-249.
96. Weksberg R, Shuman C, Beckwith JB: **Beckwith-Wiedemann syndrome**. *Eur J Hum Genet* 2010, **18**(1):8-14.
97. Tan TY, Amor DJ: **Tumour surveillance in Beckwith-Wiedemann syndrome and hemihyperplasia: a critical review of the evidence and suggested guidelines for local practice**. *J Paediatr Child Health* 2006, **42**(9):486-490.
98. DeBaun MR, Siegel MJ, Choyke PL: **Nephromegaly in infancy and early childhood: a risk factor for Wilms tumor in Beckwith-Wiedemann syndrome**. *J Pediatr* 1998, **132**(3 Pt 1):401-404.
99. Mussa A, Molinatto C, Baldassarre G, Riberi E, Russo S, Larizza L, Riccio A, Ferrero GB: **Cancer Risk in Beckwith-Wiedemann Syndrome: A Systematic Review and Meta-Analysis Outlining a Novel (Epi)Genotype Specific Histotype Targeted Screening Protocol**. *J Pediatr* 2016, **176**:142-149.e141.
100. Quarello P, Carli D, Biasoni D, Gerocarni Nappo S, Morosi C, Cotti R, Garelli E, Zucchetti G, Spadea M, Tirtei E *et al*: **Implications of an Underlying Beckwith-Wiedemann Syndrome for Wilms Tumor Treatment Strategies**. *Cancers (Basel)* 2023, **15**(4).
101. Turner JT, Hill DA, Dome JS: **Revisiting the Threshold for Cancer Genetics Referral in Patients With Wilms Tumor**. *J Clin Oncol* 2022, **40**(17):1853-1860.
102. Shieh HF, Estroff JA, Barnewolt CE, Zurakowski D, Tan WH, Buchmiller TL: **Prenatal imaging throughout gestation in Beckwith-Wiedemann syndrome**. *Prenat Diagn* 2019, **39**(9):792-795.

103. Williams DH, Gauthier DW, Maizels M: **Prenatal diagnosis of Beckwith-Wiedemann syndrome**. *Prenat Diagn* 2005, **25**(10):879-884.
104. Dumba M, Jawad N, McHugh K: **Neuroblastoma and nephroblastoma: a radiological review**. *Cancer Imaging* 2015, **15**(1):5.
105. Dumba M, Jawad N, McHugh K: **Neuroblastoma and nephroblastoma: an overview and comparison**: Cancer Imaging. 2014 Oct 9;14(Suppl 1):O15. doi: 10.1186/1470-7330-14-S1-O15. eCollection 2014.
106. van der Beek JN, Watson TA, Nievelstein RAJ, Brisse HJ, Morosi C, Lederman HM, Coma A, Gavra MM, Vult von Steyern K, Lakatos K *et al*: **MRI Characteristics of Pediatric Renal Tumors: A SIOP-RTSG Radiology Panel Delphi Study**. *J Magn Reson Imaging* 2022, **55**(2):543-552.
107. Sandberg JK, Chi YY, Smith EA, Servaes S, Hoffer FA, Mullen EA, Perlman EJ, Tornwall B, Ehrlich PF, Geller JI *et al*: **Imaging Characteristics of Nephrogenic Rests Versus Small Wilms Tumors: A Report From the Children's Oncology Group Study AREN03B2**. *AJR Am J Roentgenol* 2020, **214**(5):987-994.
108. Morin CE, Artunduaga M, Schooler GR, Brennan RC, Khanna G: **Imaging for Staging of Pediatric Abdominal Tumors: An Update, From the AJR Special Series on Cancer Staging**. *AJR Am J Roentgenol* 2021, **217**(4):786-799.
109. Chung EM, Lattin GE, Jr., Cube R, Lewis RB, Marichal-Hernández C, Shawhan R, Conran RM: **From the archives of the AFIP: Pediatric liver masses: radiologic-pathologic correlation. Part 2. Malignant tumors**. *Radiographics* 2011, **31**(2):483-507.
110. Grajo JR, Paspulati RM, Sahani DV, Kambadakone A: **Multiple Endocrine Neoplasia Syndromes: A Comprehensive Imaging Review**. *Radiol Clin North Am* 2016, **54**(3):441-451.
111. Giusti F MF, Brandi ML. Multiple Endocrine Neoplasia Type 1. 2005 Aug 31 [Updated 2022 Mar 10]. In: Adam MP, Feldman J, Mirzaa GM, et al., editors. GeneReviews® [Internet]. Seattle (WA): University of Washington, Seattle; 1993-2025. Available from: https://www.ncbi.nlm.nih.gov/books/NBK1538/, think!Close Tuwy.
112. Scarsbrook AF, Thakker RV, Wass JA, Gleeson FV, Phillips RR: **Multiple endocrine neoplasia: spectrum of radiologic appearances and discussion of a multitechnique imaging approach**. *Radiographics* 2006, **26**(2):433-451.
113. Walls GV: **Multiple endocrine neoplasia (MEN) syndromes**. *Semin Pediatr Surg* 2014, **23**(2):96-101.
114. Johnson NA, Tublin ME, Ogilvie JB: **Parathyroid Imaging: Technique and Role in the Preoperative Evaluation of Primary Hyperparathyroidism**. *American Journal of Roentgenology* 2007, **188**(6):1706-1715.
115. Ali A, Revels J, Wang DT, Wang LL, Wang SS: **Multimodality Imaging Review of Multiple Endocrine Neoplasia**. *AJR Am J Roentgenol* 2021, **217**(1):245-256.
116. Chaudhary V, Bano S: **Imaging of the pituitary: Recent advances**. *Indian J Endocrinol Metab* 2011, **15 Suppl 3**(Suppl3):S216-223.
117. Lee DW, Kim MK, Kim HG: **Diagnosis of Pancreatic Neuroendocrine Tumors**. *Clin Endosc* 2017, **50**(6):537-545.
118. Thakker RV: **Multiple endocrine neoplasia type 1 (MEN1)**. *Best Pract Res Clin Endocrinol Metab* 2010, **24**(3):355-370.

119. Schieda N, Siegelman ES: **Update on CT and MRI of Adrenal Nodules**. *American Journal of Roentgenology* 2017, **208**(6):1206-1217.
120. Pacak K, Eisenhofer G, Ilias I: **Diagnosis of pheochromocytoma with special emphasis on MEN2 syndrome**. *Hormones (Athens)* 2009, **8**(2):111-116.
121. Leung K, Stamm M, Raja A, Low G: **Pheochromocytoma: The Range of Appearances on Ultrasound, CT, MRI, and Functional Imaging**. *American Journal of Roentgenology* 2013, **200**(2):370-378.
122. Taïeb D, Hicks RJ, Hindié E, Guillet BA, Avram A, Ghedini P, Timmers HJ, Scott AT, Elojeimy S, Rubello D *et al*: **European Association of Nuclear Medicine Practice Guideline/Society of Nuclear Medicine and Molecular Imaging Procedure Standard 2019 for radionuclide imaging of phaeochromocytoma and paraganglioma**. *Eur J Nucl Med Mol Imaging* 2019, **46**(10):2112-2137.

FIGURES

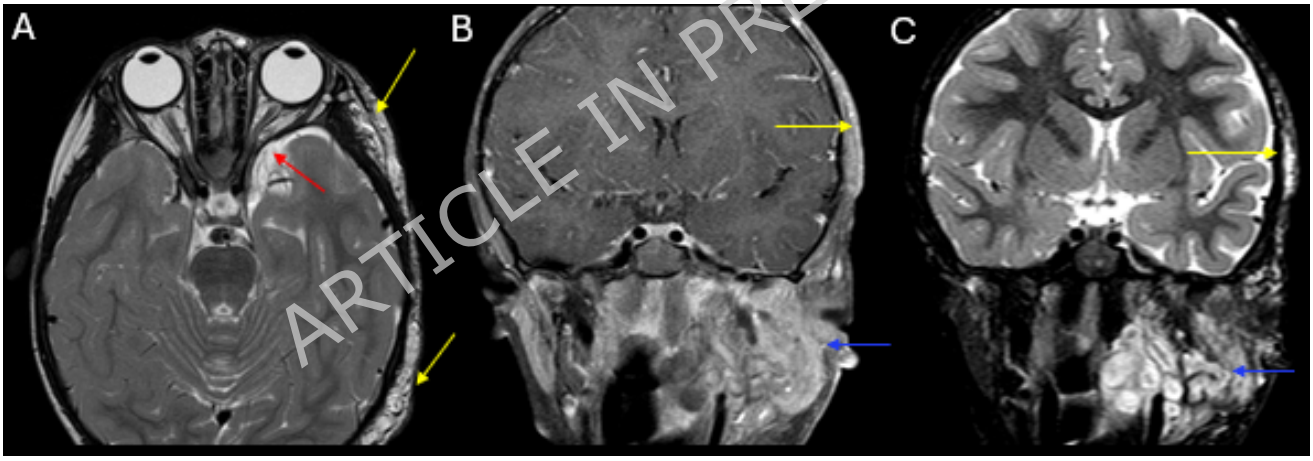

Figure 1. (A) Axial T2-weighted image of the orbits demonstrates dysplasia of the left greater wing of the sphenoid (red arrow). Scalp plexiform neurofibromas with hyperintense T2 signal are noted in the left temporal fossa and posterior occipito-temporal convexity (yellow arrows). (B) Axial T1 fat-suppressed image and (C) coronal STIR image of the sella region show extensive multispatial plexiform neurofibromas centered in the left

infratemporal fossa with extension into the parapharyngeal space, masticator space and periauricular region with enhancement and hyperintense STIR (blue arrows in B and C). There is classic “target sign” within the neurofibroma (blue arrow in C).

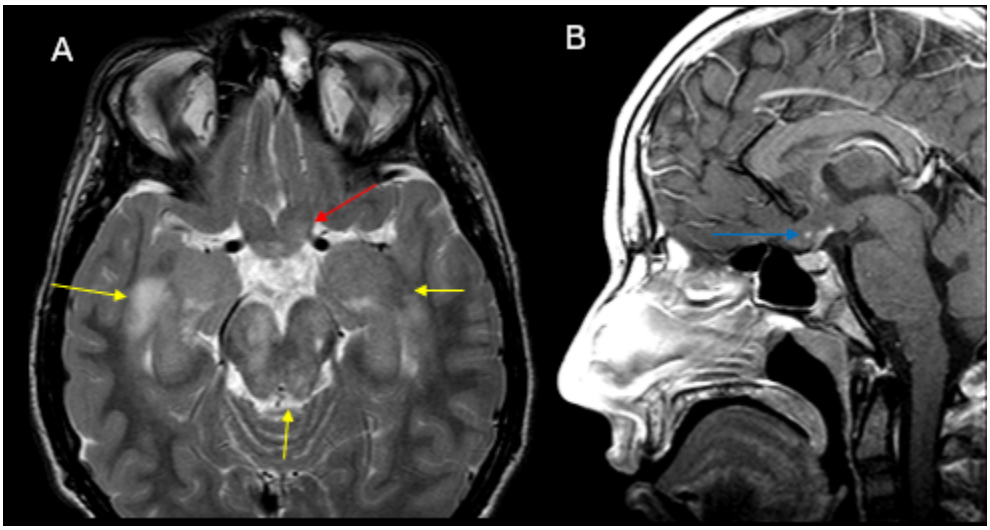

Figure 2. (A) Axial T2-weighted image of the orbits shows abnormal thickening of optic chiasm and pre-chiasmatic optic nerves with abnormal hyperintense T2 signal (red arrow), consistent with optic pathway glioma in this NF1 patient. Multifocal areas of spongiform myelin with hyperintense T2 signal are present in the bilateral medial temporal lobes and brainstem (yellow arrows). (B) Sagittal T1-weighted image of the sella redemonstrates the optic pathway glioma, showing minimal enhancement in the chiasmatic component (blue arrow in B).

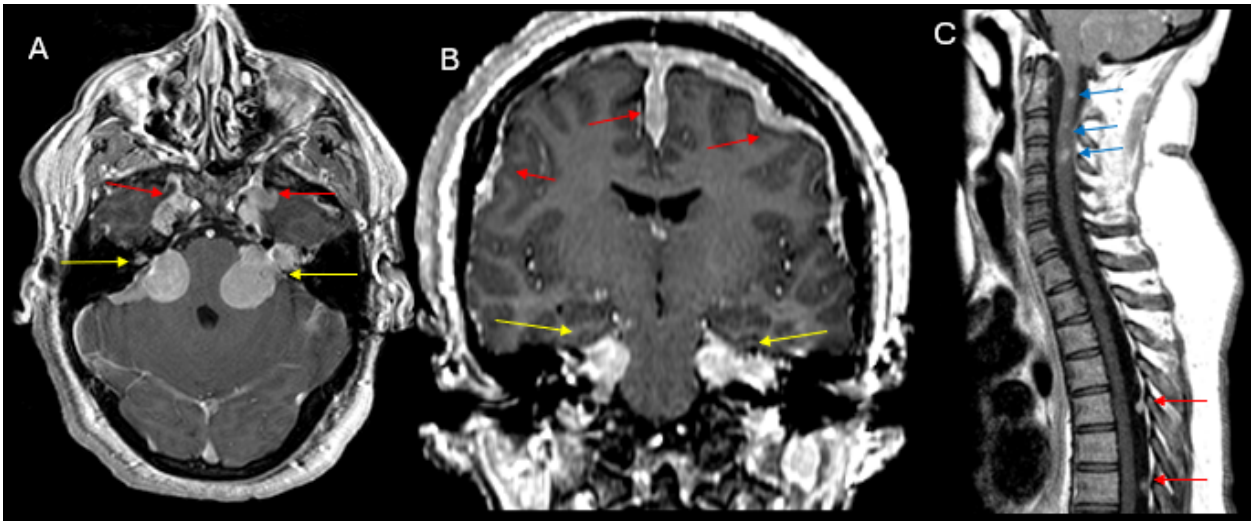

Figure 3. (A) Post-contrast axial T1-weighted and (B) coronal T1-weighted images demonstrate enhancing bilateral vestibular schwannomas (yellow arrows) and multifocal meningiomas along the cerebral convexity, falx, and bilateral mesial temporal regions (red arrows) in a patient with NF2. (C) Post-contrast sagittal T1-weighted image of the cervical and upper thoracic spine shows a few enhancing intramedullary lesions in the cervical cord, suggestive of ependymomas (blue arrows). Additionally, dural based intraspinal extramedullary lesions in the dorsal mid thoracic spine are also present, compatible with meningiomas (red arrows).

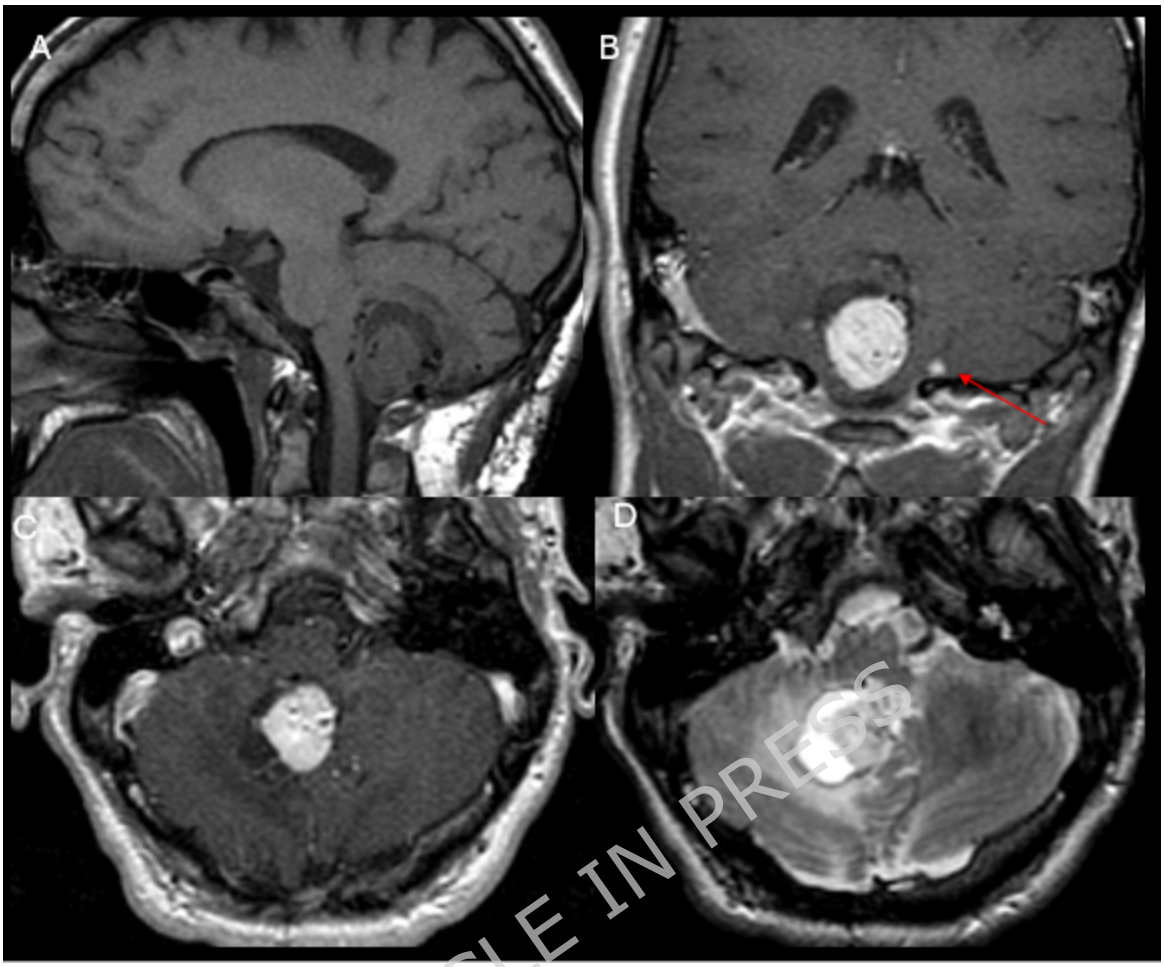

Figure 4. (A) Pre-contrast sagittal T1-weighted image (WI), (B and C) post-contrast coronal and axial T1WI and (D) Axial T2WI. There is a mild enhancing intra-axial mass in the right paramedian inferior cerebellum with associated small cysts and associated perilesional vasogenic edema demonstrating T2 hyperintensity. In addition, a small homogeneously enhancing nodule is present in the inferior aspect of the left cerebellum (red arrow in B). Multiple dilated vessels are noted along the tumor secondary to the characteristic high vascularity of the tumor. These findings are consistent with hemangioblastomas.

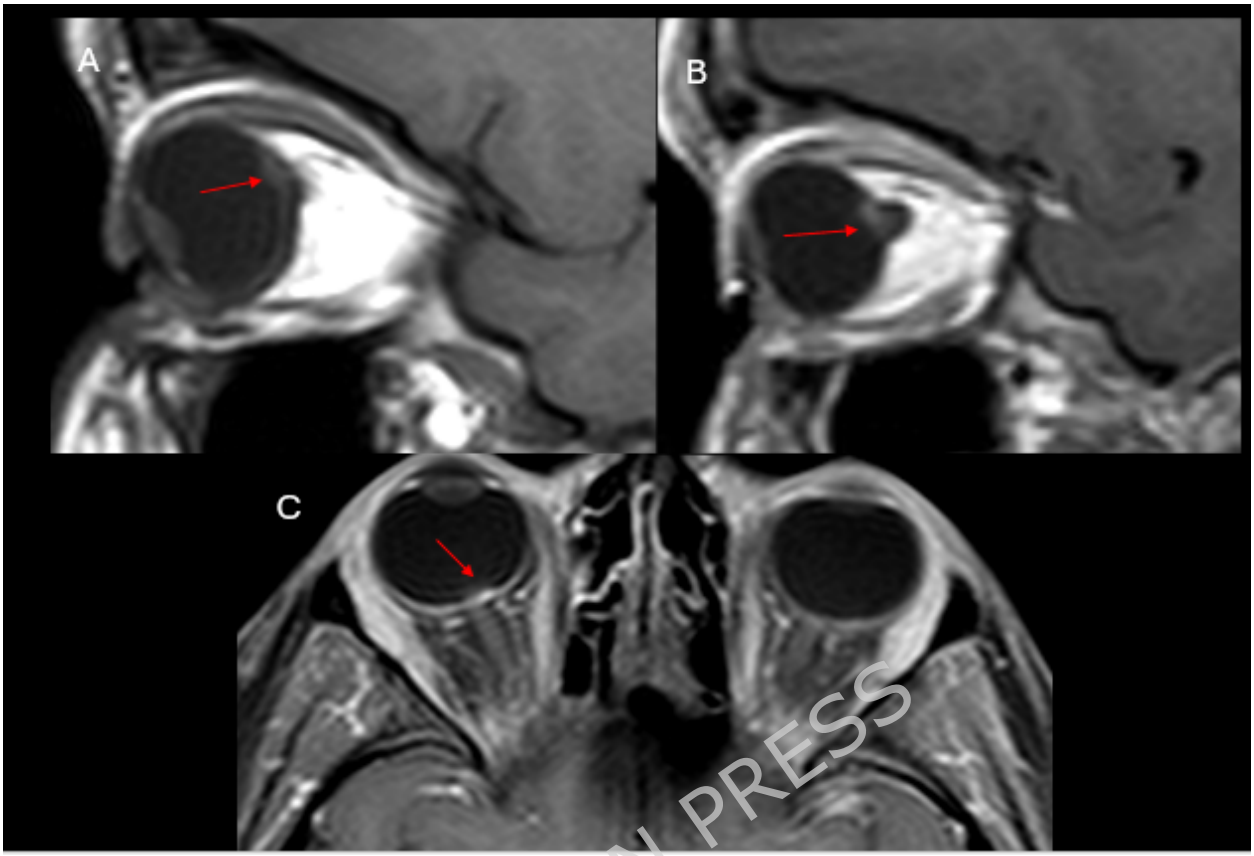

Figure 5. (A) Pre-contrast sagittal T1-weighted image (WI), (B) post-contrast sagittal T1WI, and (C) post-contrast axial T1-fat saturated (C) of the orbits demonstrate a small enhancing lesion in the nasal aspect of the right optic disc. It is consistent with retinal hemangioblastoma in this patient with history of Von Hippel Lindau syndrome.

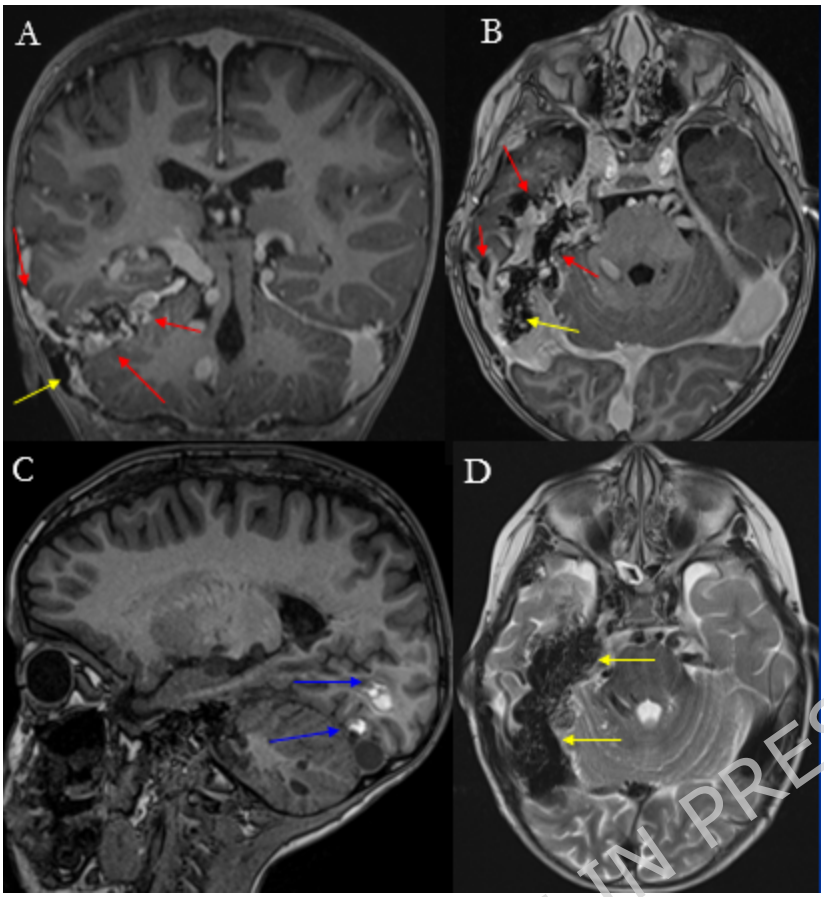

Figure 6. Child with PTEN Hamartoma Tumor Syndrome/Cowden syndrome. (A and B) Post-contrast coronal and axial T1-weighted image (WI), (C) pre-contrast sagittal T1WI, and (D) axial T2WI. There are many small dural fistulas (in the floor of the right middle cranial fossa, posterior fossa and along the tentorial leaflet with curvilinear vascular enhancement due combination of feeding arterial branches from posterior cerebral artery and inferior middle cerebral artery division branches and draining veins (red arrows in A and B) in conjunction with dilated dural sinuses. Post embolization changes with hypointense coiling materials are also noted (yellow arrows in A, B and C). Additionally, two small cavernomas with

hyperintense T1 subacute hemorrhage are present in the occipital lobe on the right (blue arrows in C).

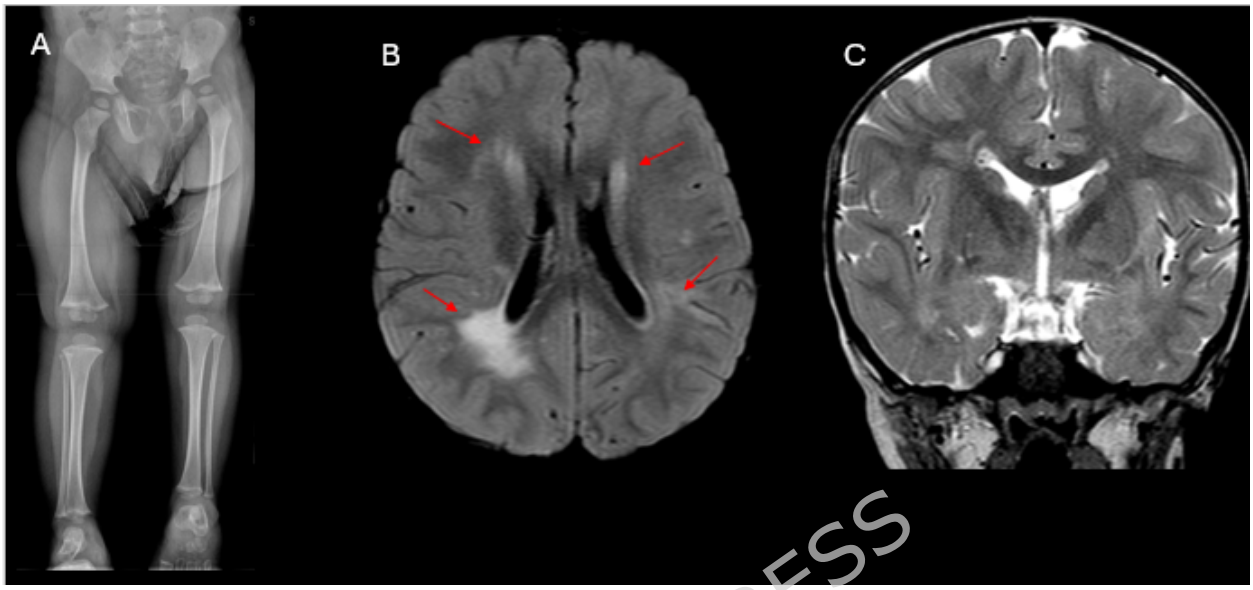

Figure 7. Child with Beckwith-Wiedemann Syndrome. (A) Leg length radiograph demonstrates leg length discrepancy, with left lower extremity shorter than the right, and hypertrophy of the right lower extremity. (B) Axial FLAIR and (C) coronal T2-weighted images show asymmetric enlargement of the right cerebral hemisphere, consistent with right hemimegalencephaly. Additionally, abnormal T2 and FLAIR hyperintense gliosis is present in the periventricular white matter bilaterally (red arrows B).

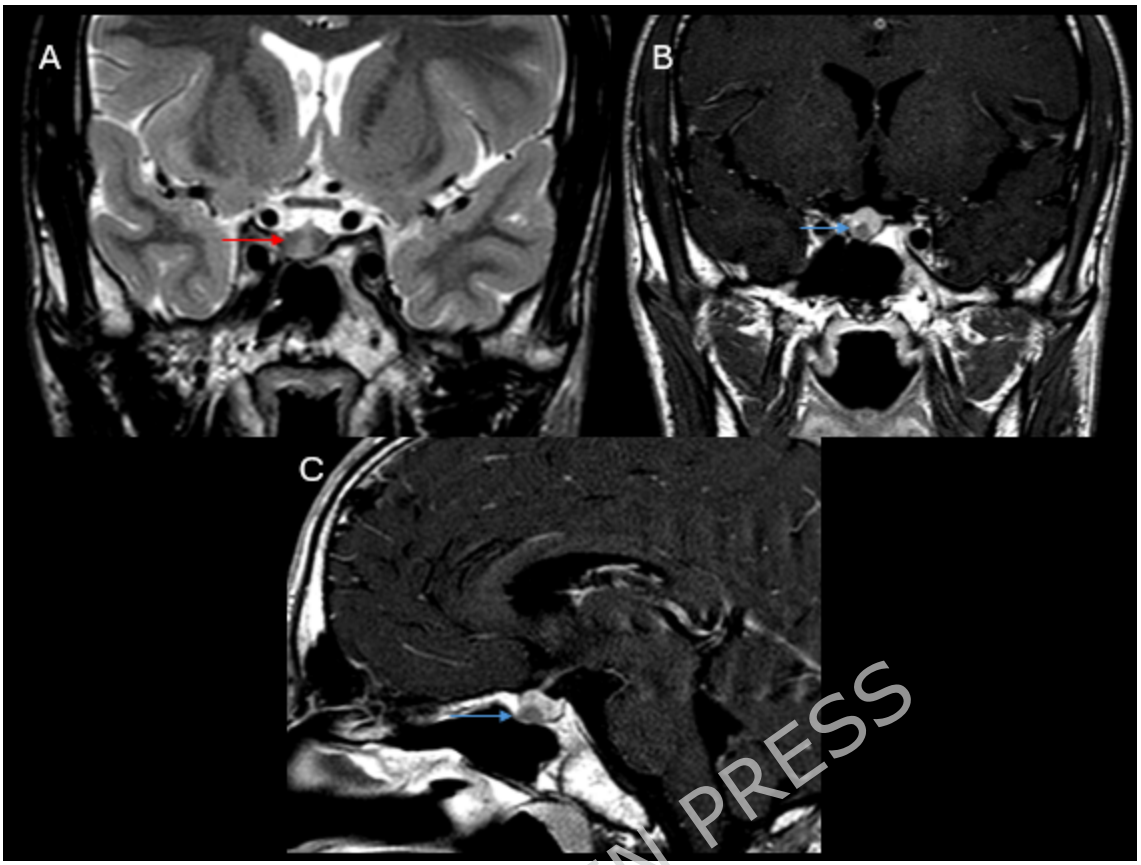

Figure 8. Patient with multiple endocrine neoplasia 1 with recurrent microadenoma. (A) Coronal T2-weighted image (WI), and post-contrast coronal (B) and sagittal (C) T1WI demonstrate a small well-circumscribed hypoenhancing nodule in the inferior adenohypophysis near the floor of the sella turcica (blue arrows in B and C). The lesion is hyperintense on T2 WI (red arrow in A), consistent with small pituitary microadenoma. There is no involvement of the cavernous sinuses or carotid arteries.